



Original Paper

# 3D Structural, Facies and Petrophysical Modeling of C Member of Six Hills Formation, Komombo Basin, Upper Egypt

Moamen Ali <sup>1,4</sup>, Ahmed Abdelmaksoud,<sup>1</sup> M. A. Essa,<sup>1</sup> A. Abdelhady,<sup>2</sup> and M. Darwish<sup>3</sup>

Received 10 June 2019; accepted 20 October 2019  
Published online: 1 November 2019

Two main reservoirs are producing in Komombo Basin: the first one belongs to the C Member of the Six Hills Formation, and the second belongs to the Albian/Cenomanian cycle. The C Member reservoir lacks detailed studies. Therefore, a detailed study of this reservoir is needed. 3D geological reservoir modeling of the C Member reservoir can be a pertinent part of an overall strategy for the development of hydrocarbon fields in Komombo Basin. Five boreholes, three vertical seismic profiles and twenty 2D seismic reflection sections are integrated in Petrel™ modeling software for building 3D structural, facies and petrophysical models for the C Member reservoir. The constructed 3D structural model reveals the presence of two normal faults, in NW–SE and NE–SW directions. A detailed petrophysical evaluation was performed for the available wells. The resulted facies/petrophysical parameters are then used as input in the processes of facies and petrophysical modeling. The C Member reservoir exhibits thickness values ranging from about 91.5 to 426.5 m. The constructed 3D facies model of the studied reservoir depicts that the shale beds have the large probability distribution in the study area with the comparison of the sandstone and siltstone beds. The created 3D petrophysical models reveal that the C Member reservoir has a fair reservoir quality. This reservoir exhibits, generally, high water saturation values in most parts of the study area, while the hydrocarbon saturation is restricted to the depocenter of the basin.

**KEY WORDS:** Komombo Basin, C Member, Six Hills Formation, Reservoir characterization, 3D geological model, Upper Egypt.

## INTRODUCTION

Rift basins are considered the most important and primary targets for hydrocarbon exploration in North Africa (Nagati 1986; Meshref 1990; Ali et al.

2019a). Aeromagnetic and gravity data revealed the presence of elongated low structural areas in the southern part of the Western Desert. These areas were interpreted as half-graben basins. The Komombo Basin in the Western Desert and Nuqura and Kharit Basins in the Eastern Desert represent examples for these half-graben rift basins (Klitzsch 1984; Wycisk 1987; Meshref 1990; Taha and Aziz 1998). These grabens lack detailed studies, so their evaluation is very necessary because it will provide much useful information about the hydrocarbon potential in these basins (Ali et al. 2017b). Nagati

<sup>1</sup>Department of Geology, Faculty of Science, Assiut University, Assiut 71516, Egypt.

<sup>2</sup>DEA Group, Cairo, Egypt.

<sup>3</sup>Department of Geology, Faculty of Science, Cairo University, Giza 12613, Egypt.

<sup>4</sup>To whom correspondence should be addressed; e-mail: momen.mohamed@science.au.edu.eg

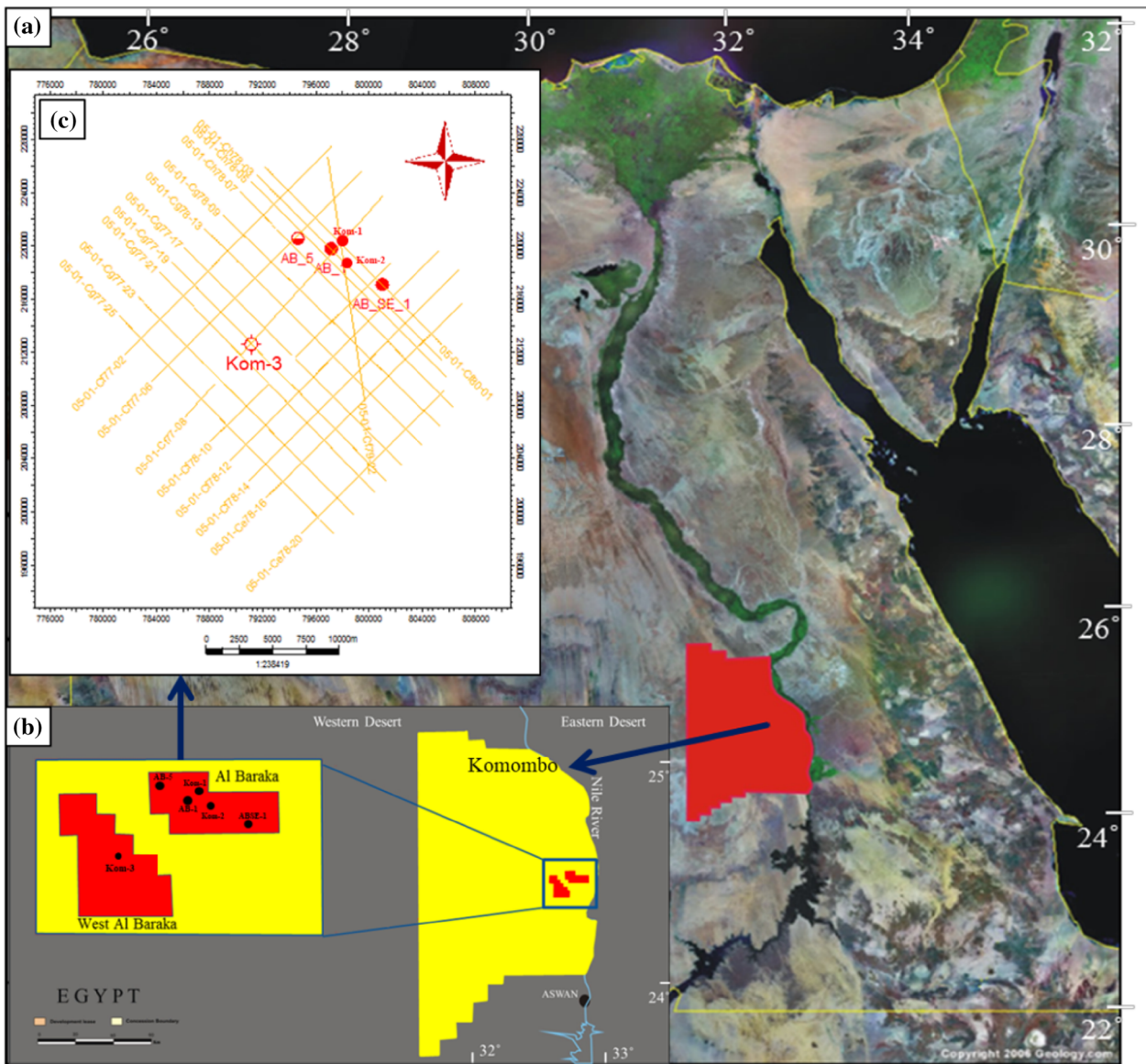


**Figure 1.** (a) Landsat image (MDA Federal 2004) showing the study area within Komombo Basin, Southern Egypt (Ali et al. 2017b). (b) and (c) Base maps showing the location of the used boreholes and twenty 2D seismic lines.

(1986) was the first to point out the presence of hydrocarbons in Upper Egypt. He discussed the presence of a triple junction in Upper Egypt. He identified and pointed out the presence of the Mesozoic rift basins in Upper Egypt from the interpretation of the aeromagnetic data.

The Komombo Basin lies in the southern part of the Western Desert, approximately 65 km northwest of Aswan city (Fig. 1a). It represents a half-graben and an intracontinental rift basin

(Fig. 2); it is the only hydrocarbon-producing basin in southern Egypt (Ali et al. 2017a). Therefore, the authors aim to conduct a detailed study of the main structural elements and to discuss the characteristics of the main reservoirs of the Komombo Basin that have not been studied previously, as well as they have studied the main source rocks in this basin (Ali et al. 2018, 2019b).

The C Member reservoir is one of the two main reservoirs that contribute to the petroleum system in

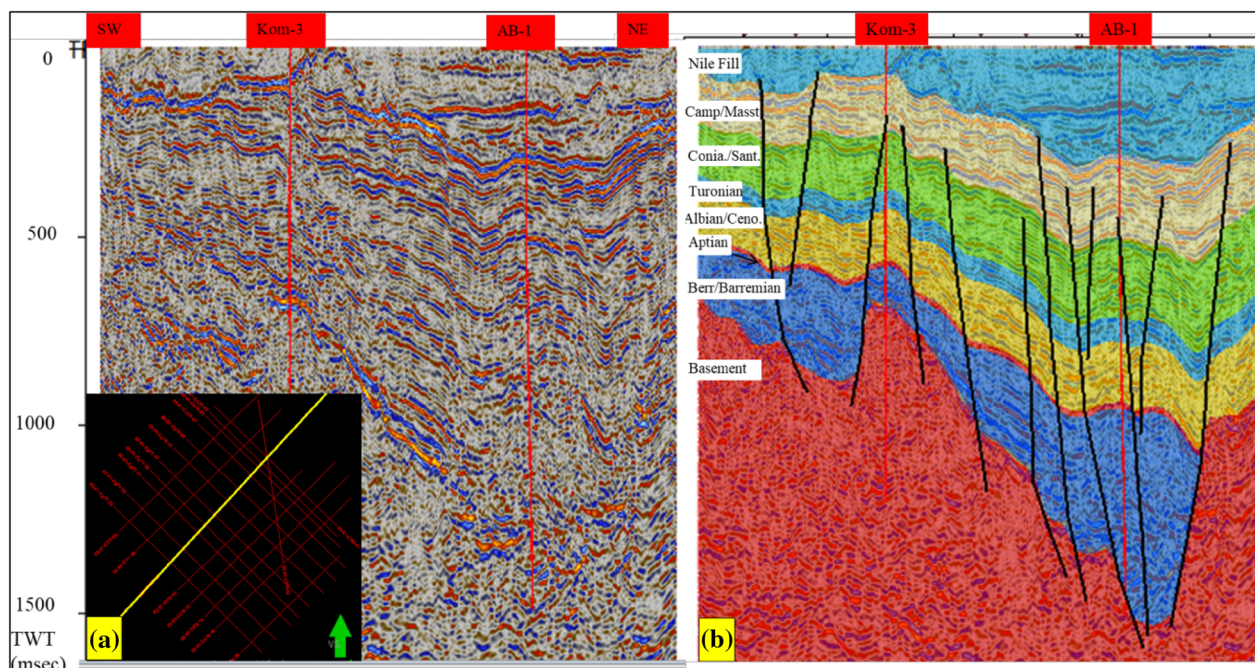


**Figure 2.** (a) Un-interpreted NE–SW 2D seismic section (05-01-Cf77-08) crossing the Komombo Basin, Upper Egypt. (b) Interpreted NE–SW 2D seismic section showing the half-graben basin and the main seismic horizons in the study area (Ali et al. 2019).

the Komombo Basin (Ali 2017). This reservoir has not been studied previously in detail. Therefore, the main objective of the current research is the integration of the available data (represented mainly by 2D seismic reflection sections, wireline logs and the description of ditch samples) to identify the main structural features of the study area, to recognize the thickness/facies distribution of the C Member reservoir and to evaluate the studied reservoir from the petrophysical point of view. This work represents a 3D geological modeling approach, comprising 3D structural, facies and petrophysical models.

The main character of the 3D geomodeling techniques is the ability to model complex structures. This technique allows the interpreter to evaluate the model by displaying cross sections along any direction through the constructed model. The concept of 3D facies/petrophysics is also essential for linking wellbore measurements to a 3D geological model (Bryant and Flint 1993; Bilodeau et al. 2002; Cosentino 2005; De Jager and Pols 2006; Abdel-Fattah et al. 2010; Abdelmaksoud et al. 2019a, b).

## GEOLOGICAL SETTING

The Komombo Basin was formed due to the stress regime created in North and Central Africa that was associated with the opening of the South Atlantic. This basin is bounded by a major normal fault striking NW–SE that is situated on the NE side of the Komombo Basin and downthrown to the southwest. There are also many minor normal faults with the same NW–SE direction. The Komombo Basin contains great sedimentary cover of about 4000 m (Fig. 3). This cover is composed mainly of clastics (shale and sandstone) with some carbonate deposits (Ziegler 1992; Bosworth et al. 2008). The Komombo Basin holds two oil fields, Al Baraka and West Al Baraka fields (Fig. 1b). It is a great exploration target for GANOPE and DANA petroleum companies because most of the previous work and exploration activities until the 1990s concentrated on the unstable shelf in the northwestern desert where thick marine Cretaceous and Jurassic sediments were identified (Ali et al. 2019b).

The stratigraphic column of the Komombo Basin is representative of non-marine and shallow

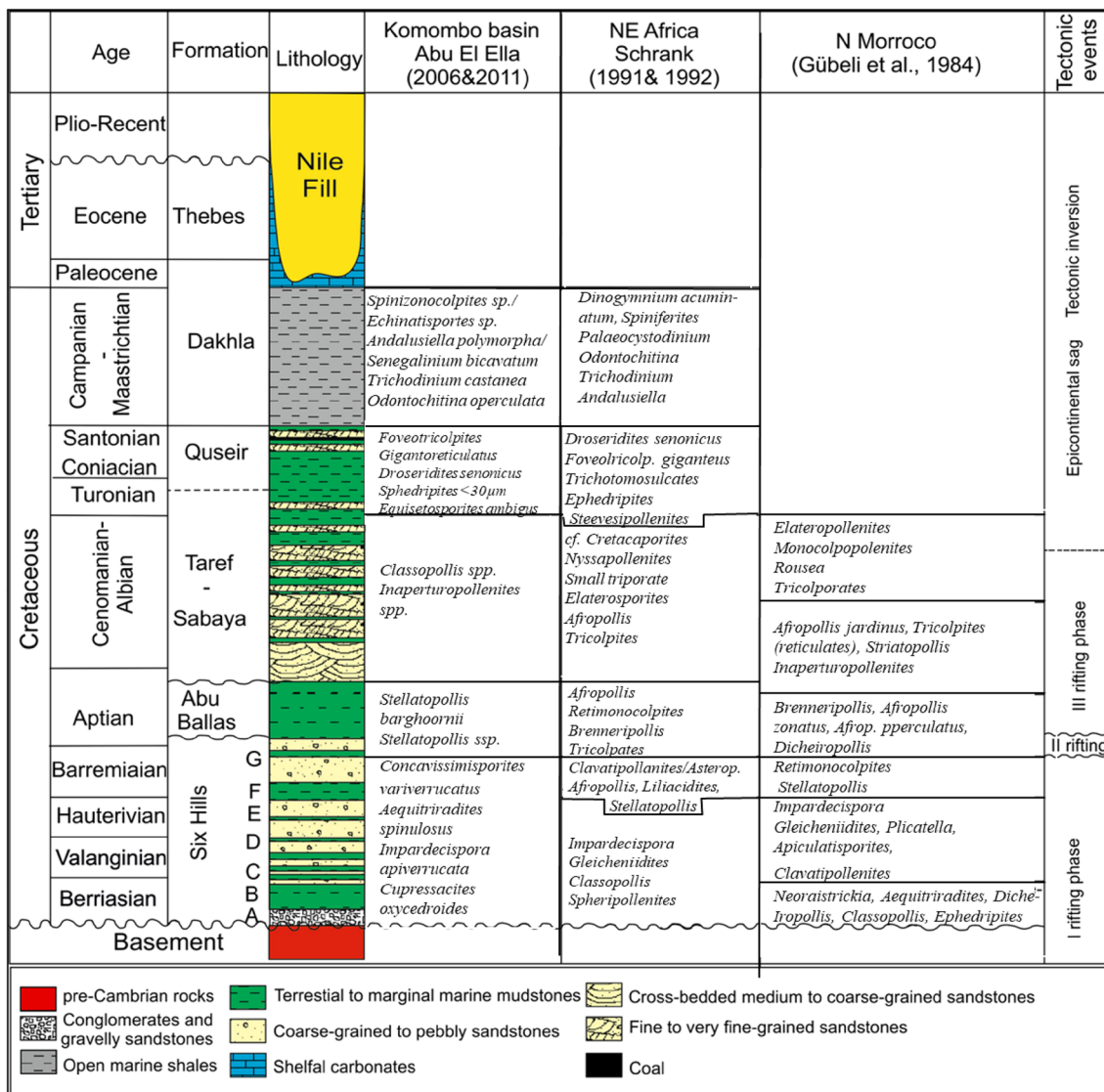


Figure 3. Stratigraphic chart of the Komombo Basin, showing that the stratigraphic succession is representative of non-marine and shallow marine deposits are during the Cretaceous (Selim 2016).

marine sequences deposited during the Cretaceous (Abdelhady et al. 2016). The stratigraphic succession is composed of seven formations, namely from top to bottom, Dakhla, Qusier, Taref, Maghrabi, Sabaya, Abu Ballas and Six Hills Formations (Fig. 3). The Six Hills Formation composed of a succession of fining-up cycles, medium- to coarse-grained sandstone and described as fluvial deposits. The sandstone exhibits large-scale tabular planar cross-bedding sets (Klitzsch et al. 1979; Hendriks et al.

1984). It belongs to Late Jurassic–Early Cretaceous with type section between Six Hills and Gebel Nusb el-Balgum, northeast of Bir Tarfawi (Barthel and Boettcher 1978). It classified into seven members (A–G), where A member at the bottom and G member at the top. A member composed of gravelly sandstone with some mudstone inter-beds. B member composed mainly of gray to dark gray organic-rich mudstone. C–E members consist of successive alternations of pebbly to medium-grained sandstone

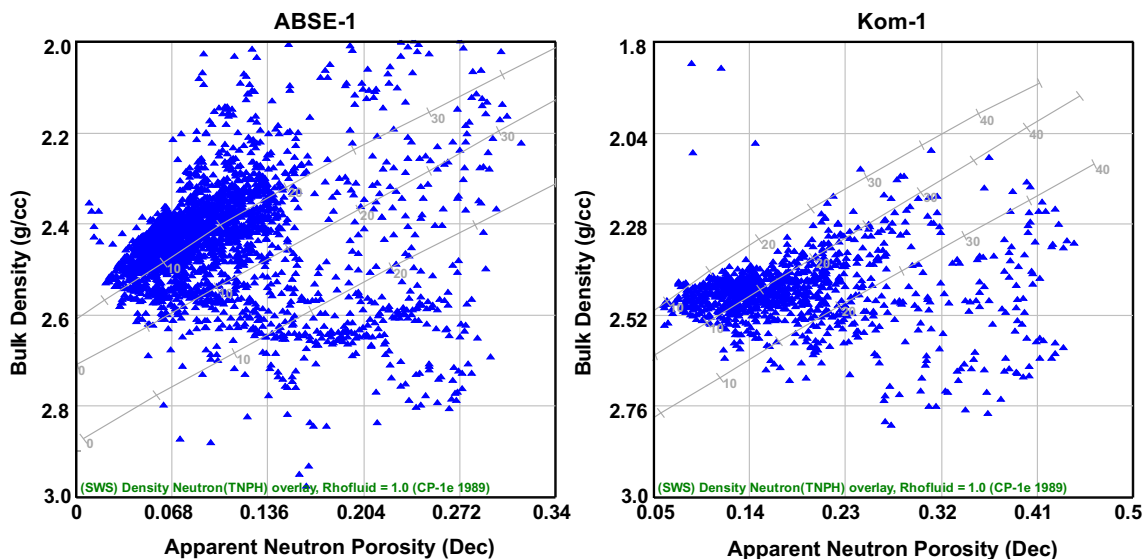


Figure 4. Neutron–density cross-plots of the C Member reservoir (example of wells ABSE-1 and Kom-1) for recognizing the comprising lithology.

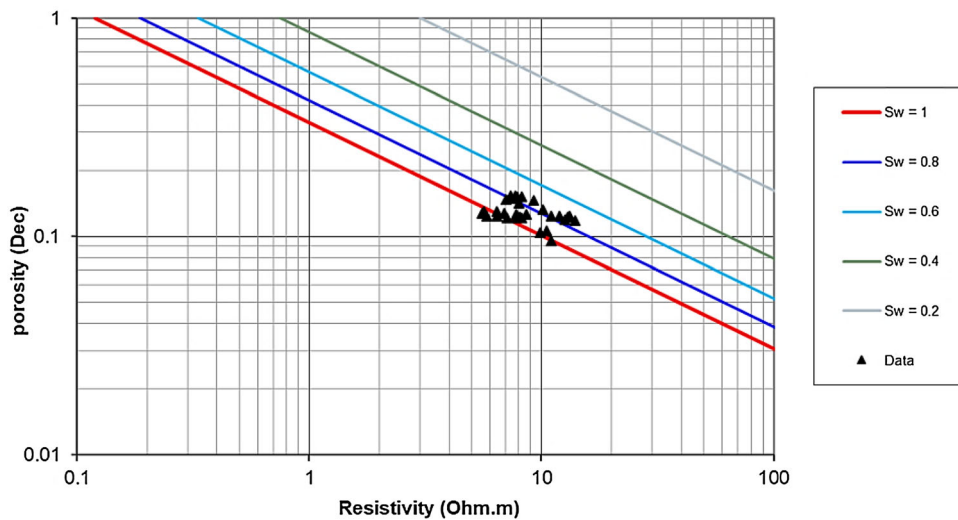


Figure 5. Pickett's plot [true resistivity ( $R_t$ ) vs. total porosity values ( $\Phi$ )] for interval 2119.7–2164 m in Kom-1 well.

and red to brown mudstone with general coarsening upward pattern. F member consists of variegated to red mudstone with thin sandstone inter-beds. G member is similar to E member but shows wide spatial distribution (Selim 2016). The C Member of the Six Hills Formation consists mainly of shale with

sandstone and siltstone streaks, deposited as fan-delta and/or fluvial deposits. The C Member reservoir represents the first siliciclastic reservoir in the Komombo Basin (Abdelhady 2016). Selim (2016) recognized the depositional environments in the Komombo Basin, and he supposed that the C

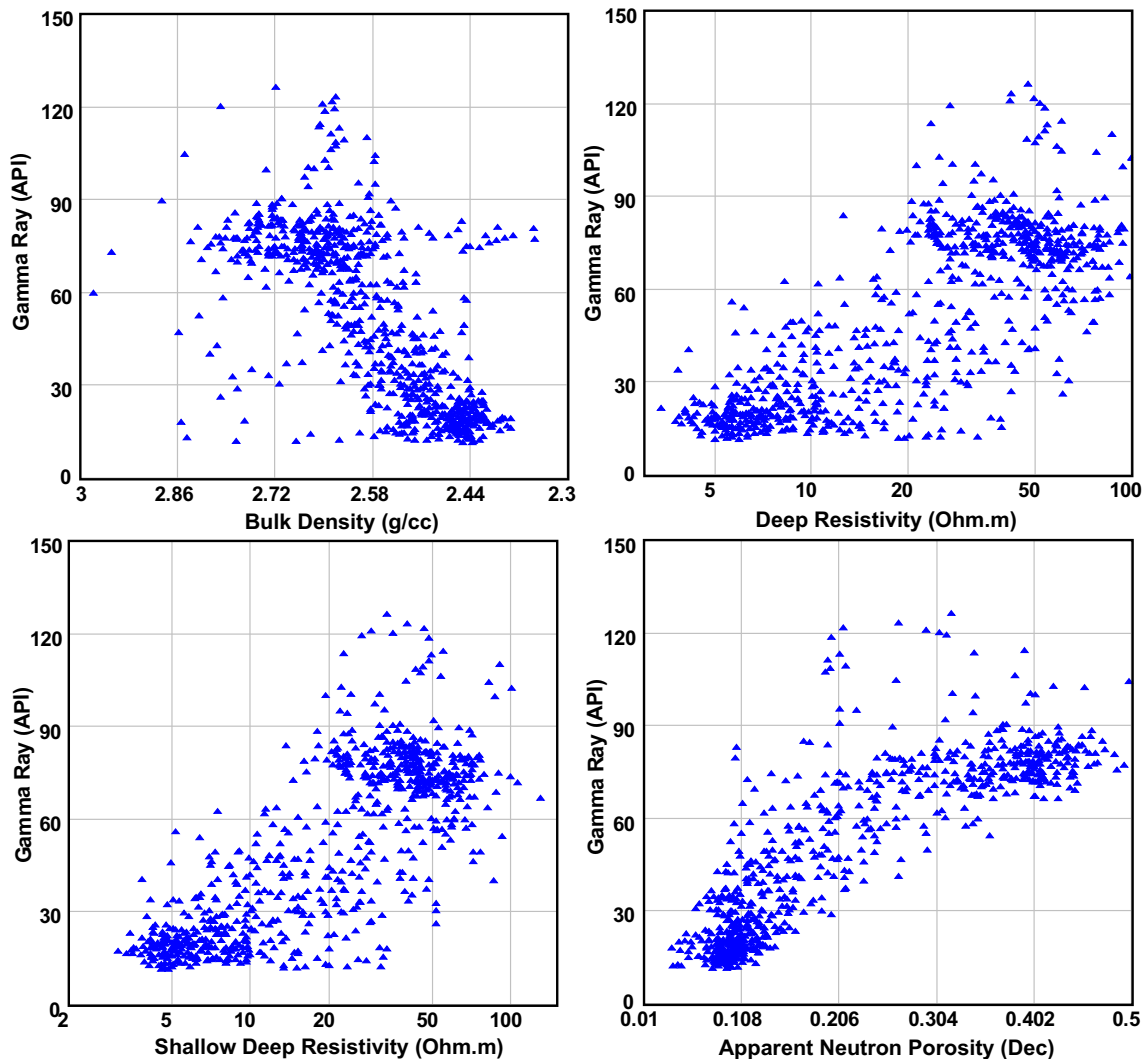


Figure 6. Cross-plotting of bulk density, apparent neutron porosity, shallow resistivity and deep resistivity values vs. gamma ray values (example of AB-1 well) for obtaining the shale parameters.

Member of the Six Hills Formation is representative by two facies associations: distal braid-plain and mid-braid-plain. The first one is characterized by red, massive to laminated mudstone with medium- to coarse-grained sandstones, exhibiting fining-upward patterns. The large probability distribution of the red mudstones in the C Member reflects the deposition under low-energy and oxidizing conditions. The mid-braid-plain facies association is characterized by semi-equal red mudstone and

coarse-grained to pebbly sandstones. The thickness of the C Member reservoir varies in the drilled wells from 165, 244, 116 and 216 m in Kom-1, Kom-2, AB-1 and ABSE-1 wells, respectively.

**MATERIALS AND METHODS**

The available data sets that are used in the present study include four well data sets (Kom-1,

Kom-2, AB-1 and ABSE-1 wells) and three vertical seismic profiles (VSP), in addition to twenty 2D seismic reflection sections. These sections are represented by eight sections with a NE trend and twelve sections with a NW-NNW trend (Fig. 1c). The data sets include the detailed description of the ditch samples of wells AB-1 and ABSE-1, as well. Authors achieved their aims by integrating the available data in Petrel™ modeling software. The present work is initiated by the interpretation of seismic data, which is subdivided into many steps, including seismic to well tying, interpreting faults and picking horizons of the top and bottom of the C Member to construct the two-way time (TWT) surface. The final step in seismic interpretation is the domain conversion of the TWT surface to depth surface using the velocity surface (Cosentino 2005; Abdelmaksoud et al. 2016, 2017). The results of the seismic interpretation are then incorporated as input data in the 3D structural modeling process. This structural model/framework acts as a container for the facies and petrophysical characteristics.

The structural modeling process is subdivided into three main processes: fault modeling, pillar gridding and making horizons. Firstly, the interpreted faults are modeled followed by the pillar gridding process, which represents the creation of structural grids from the fault model. The final process is making horizons, which represent the addition of the different layers of the model by inserting the interpreted horizons, represented by the top and bottom of the C Member reservoir (Cosentino 2005; Abdelmaksoud 2017; Abdelmaksoud et al. 2019a). Petrophysical evaluation of the C Member is then conducted, where the various petrophysical characteristics are obtained through the analyses of the different well logging curves. The

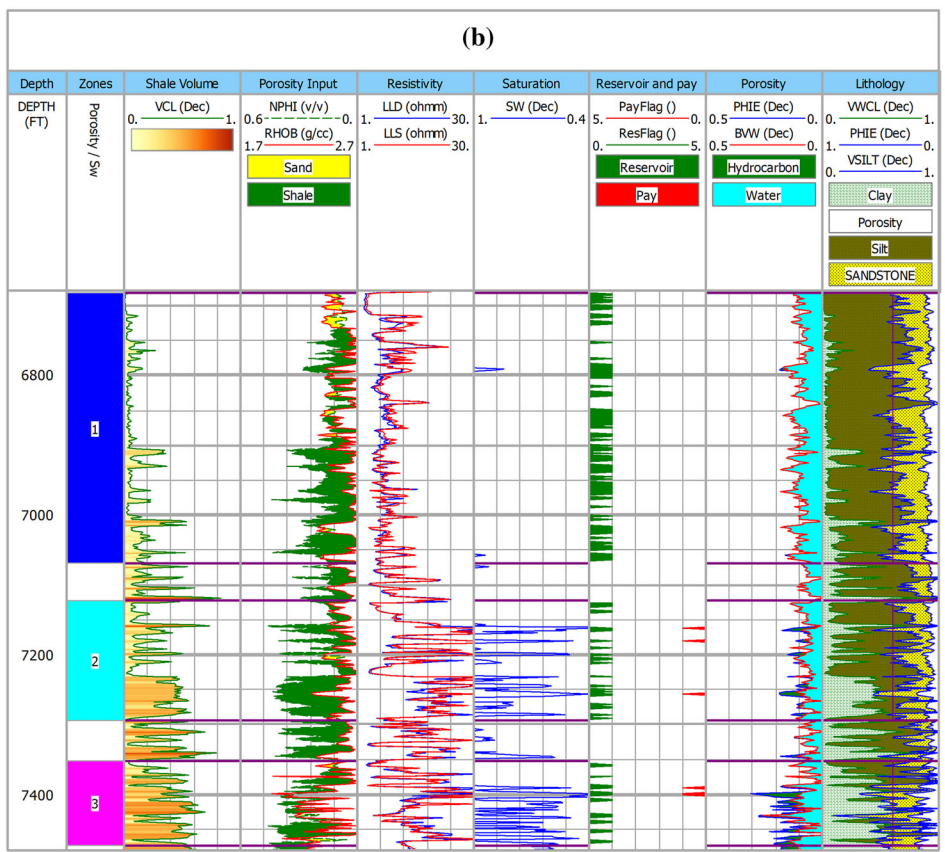
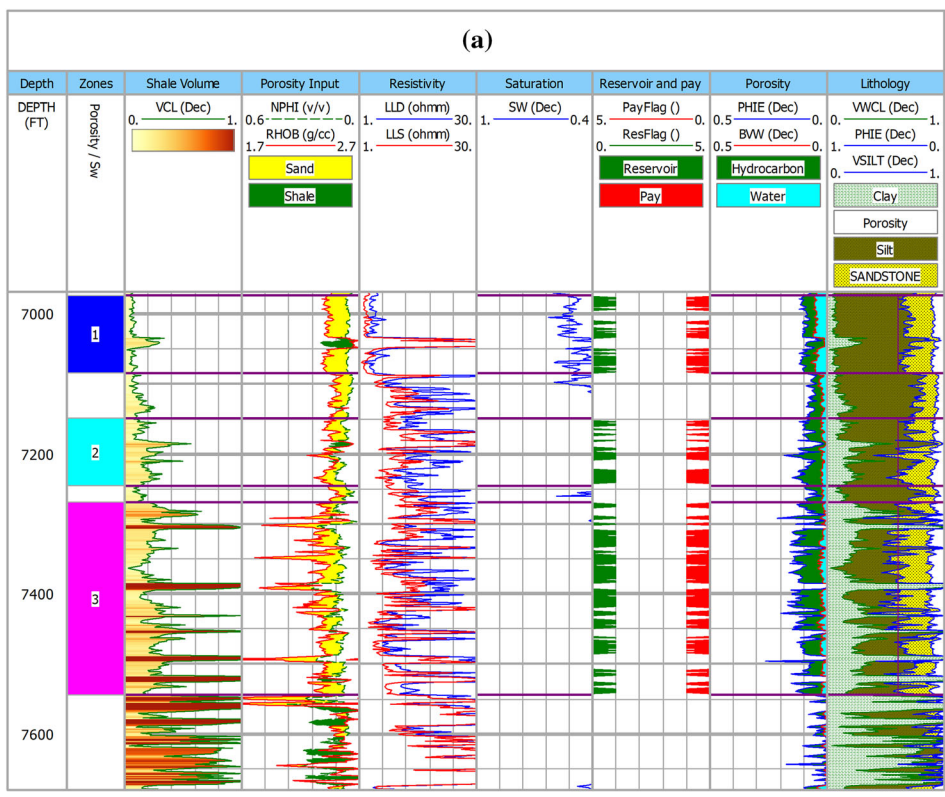
lithological interpretation of the C Member reservoir is based on the description of the ditch samples in addition to the different well logs, i.e., caliper, resistivity, gamma ray and sonic logs in addition to neutron-density cross-plots (Fig. 4).

The petrophysical evaluation is initiated with the quantitative interpretation of the well logging data. The water resistivity ( $R_w$ ) is calculated using the spontaneous potential log ABSE-1 well and is found to equal 0.12  $\Omega$  m at the formation temperature (85 °C). The relationship between the true resistivity and total porosity of Pickett's plot (Pickett 1972) is used for determining cementation factor ( $m$ ) of the C Member reservoir (Fig. 5). Simply, the cementation factor of the reservoir can be obtained from the slope of the line, which has 100% water saturation. The slope of this line equals to  $-m$ . The obtained cementation factor value equals 1.93 for C Member. Determination of shale parameters and taking into account their effects on the well log measurements is one of the most important steps in well log analysis. These parameters are represented in the present study by the resistivity of shale ( $R_{sh}$ ), neutron porosity of shale ( $\Phi_{Nsh}$ ) and density of shale ( $\rho_{sh}$ ). These parameters can be obtained from the cross-plots of gamma ray values vs. bulk density, apparent neutron porosity, shallow resistivity and deep resistivity values (Fig. 6). The equation of Larionov (1969) for older rocks is applied on the gamma ray log in order to calculate the clay volume ( $V_{cl}$ ) of the studied reservoir. Both the neutron and density logs are used in calculating the total and effective porosities ( $\Phi_t$  and  $\Phi_e$ , respectively) of the studied reservoir. The water saturation ( $S_w$ ) is estimated using the Indonesian equation (Poupon and Leveaux 1971) because the studied reservoir contains variable amounts of clay. The hydrocarbon saturation ( $S_h$ ) is calculated by subtracting  $S_w$  from 100% saturation.

In order to get approximate values for permeability (K), the Timur equation (Timur 1968) is used. Although empirical estimates of permeability have uncertainties, the Timur equation has the lowest. The irreducible water saturation ( $S_{wi}$ ) values are set to 0.01 below the lowest water saturation noticed anywhere in the reservoir in logs (Darling 2005; Abdelmaksoud 2017; Abdelmaksoud et al. 2019b).

**Table 1.** Estimated shale parameters of the C Member reservoir in the studied wells

Well	Parameter		
	$R_{sh}$ ( $\Omega$ m)	$\rho_{sh}$ (gm/cc)	$\Phi_{Nsh}$ (%)
ABSE-1	20.50	2.50	20.7
AB-1	47.00	2.64	25.50
Kom-1	18.00	2.40	35.00
Kom-2	18.25	2.44	34.00





◀ **Figure 7.** Examples of litho-saturation cross-plots of the C Member reservoir: (a) ABSE-1 well; (b) Kom-2 well.

Cutoff values are used for obtaining the net reservoir and pay thicknesses. These values are 40% for shale volume, 10% for porosity and 60% for water saturation. The next stage in reservoir modeling is the population of the reservoir rock's facies/petrophysical characteristics, such as porosity, permeability and facies directly from well data, through the 3D model. The obtained lithologies/facies and petrophysical characteristics are therefore used as input in the previously constructed 3D structural framework in order to obtain 3D facies and petrophysical models for the C Member reservoir, through the processes of facies and petrophysical modeling.

## RESULTS AND DISCUSSION

### Lithology and Petrophysical Parameters

The lithology of the C Member reservoir is interpreted, from well logs, as sandstone cemented by argillaceous and/or calcareous materials, siltstone and shale. The obtained cross-plots exhibit three main clusters. The shale lithology is represented by the first cluster of these cross-plots. It lies in the upper portion of the cross-plots. Shale is characterized by high gamma ray readings (130–170 API), high neutron porosity (20.7–35% porosity units, pu) and relatively intermediate bulk density (2.40–2.64 gm/cc), while it exhibits intermediate, deep resistivity values (18–47  $\Omega$  m). The average shale parameters for the studied wells show that wells ABSE-1 and AB-1 have intermediate neutron porosity, relatively high density and intermediate to high resistivity, which reflects that this shale is almost dry, while wells Kom-1 and Kom-2 exhibit high neutron porosity, relatively low density and inter-

**Table 2.** A summary of the average petrophysical parameters of the C Member reservoir within the studied wells

Well	Parameter								
	Gross thickness (m)	Net reservoir (m)	Net pay (m)	Net/gross	Average $\Phi_e$ (%)	Average $V_{cl}$ (%)	Average $S_w$ (%)	Average $S_h$ (%)	Average $k$ (mD)
ABSE-1	216	68.9	68.50	0.469	12.4	18.30	25.4	74.60	65
AB-1	116	27.0	0.45	0.422	12.6	4.30	93.2	6.80	2
Kom-1	165	101.7	6.25	0.693	13.6	12.00	88.0	12.00	6
Kom-2	244	77.8	3.15	0.375	13.3	12.70	91.9	8.10	9

**Table 3.** Quantitative results of the petrophysical analysis of all identified reservoir zones in the studied wells within the C Member

Well	Zone #	Top (m)	Bottom (m)	NST (m)	NRT (m)	NPT (m)	N/G	$\Phi_e$ (%)	$V_{sh}$ (%)	$S_w$ (%)	$S_h$ (%)
ABSE-1	1	2125.29	2159.28	34.00	15.47	15.10	0.455	10.8	6.5	48.5	51.5
	2	2179.09	2208.20	29.12	11.43	11.43	0.393	11.7	19.8	21.2	78.8
	3	2215.59	2299.49	83.90	42.00	42.00	0.500	13.2	22.3	19.4	80.6
AB-1	1	2186.03	2194.41	8.38	5.18	0.46	0.618	12.5	8.3	80.0	20
	2	2219.10	2257.65	38.56	13.56	0.00	0.352	12.9	3.5	95.7	4.3
	3	2270.15	2287.07	16.92	8.23	0.00	0.486	12.3	3.1	97.3	2.7
Kom-1	1	2090.93	2110.13	19.20	13.50	2.60	0.702	13.4	5.8	83.2	16.8
	2	2114.25	2221.08	106.83	82.83	2.60	0.775	13.7	12.4	88.9	11.1
	3	2229.92	2250.49	20.58	5.34	1.10	0.259	13.1	20.3	85.5	14.5
Kom-2	1	2036.47	2154.61	118.14	53.85	0.00	0.456	12.6	7.90	99.7	0.3
	2	2170.70	2223.26	52.56	13.00	1.27	0.245	12.7	24.1	77.8	22.2
	3	2241.21	2277.70	36.49	11.00	1.88	0.302	17.2	22.8	75.7	24.3

NTS, net sand thickness; NRT, net reservoir thickness; NPT, net pay thickness; N/G, net-to-gross ratio;  $\Phi_e$ , effective porosity;  $V_{sh}$ , volume of shale;  $S_w$ , water saturation;  $S_h$ , hydrocarbon saturation

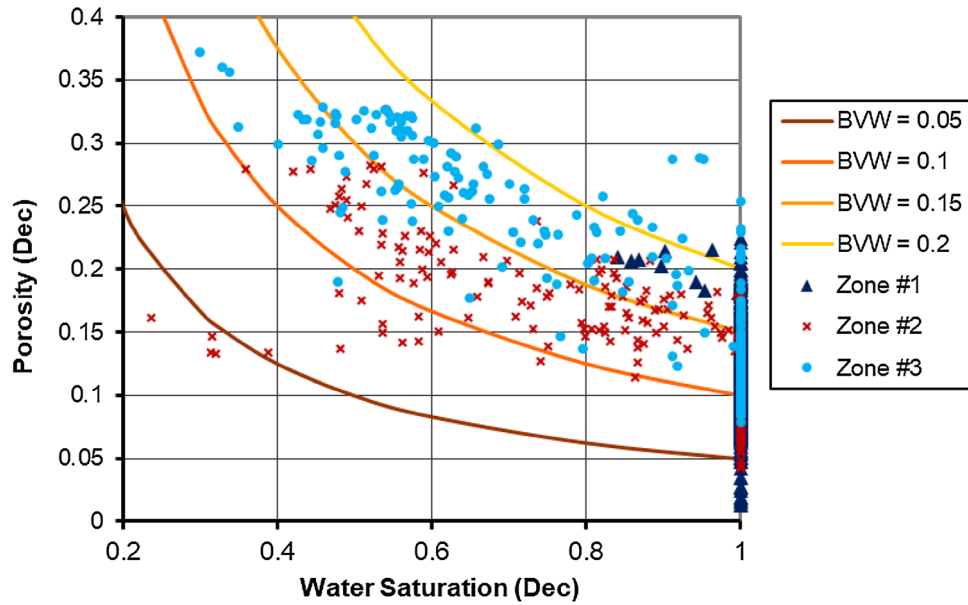


**Figure 8.** Buckles plot of porosity as a function of water saturation, indicating the bulk volume of water (example of the three zones of Kom-2).

mediate to low resistivity, indicating that most of the shales in these wells are wet (Table 1). The second cluster lies in the lower portion of these cross-plots representing sandstone lithology. The third cluster that is sandwiched between the two previous clusters represents the shaly sandstone and siltstone lithologies. The obtained petrophysical parameters of the C Member reservoir within the studied wells are presented in Figures 6 and 7 and in Table 2. Three main reservoir zones are identified through the C Member. The detailed petrophysical parameters for these zones are presented in Table 3. Kom-1 well exhibits the highest net reservoir thickness with 101.7 m, while AB-1 has the lowest value (27 m). The net pay has its greatest and smallest values in ABSE-1 (68.5 m) and AB-1 (0.45 m) wells, respectively. The four wells have approximately the same average porosity values (about 13%). The C Member reservoir zones exhibit relatively low shale content, ranging from about 3–24%. ABSE-1 is the only well with high hydrocarbon saturation values (51.5–80.6%). On the other hand, wells AB-1, Kom-1 and Kom-2 have low hydrocarbon saturation values (2.7–20%, 11.1–16.8% and 0.3–24.3%, respectively). The water saturation values can be displayed using Buckles plot (Buckles 1965) which plots porosity as a function of water saturation. Plotting

porosity as a function of water saturation is adopted by a set of hyperbolas of fixed bulk volume of water (BVW) values (Nabawy et al. 2018a). The lower the BVW values, is the better reservoir quality characterized by higher permeability, coarser grain size and much more pore connectivity (Fig. 8).

### TWT, Depth and Isopach Maps of the C Member Reservoir

The TWT contour map of the top of the C Member of the Six Hills Formation displays two main general normal fault trends in the NW–SE and NE–SW directions. The TWTs of the reservoir increase in the eastern part of the Komombo Basin, recording the maximum value of about 1600 ms, representing low structure features. The TWTs decrease in the western and southwestern parts of the Komombo Basin, recording the minimum value of about 600 and 700 ms, respectively, representing high structural features (Fig. 9).

The depth structure contour map of the top of the C Member reservoir shows that the Komombo Basin is controlled by many normal faults. These faults form horsts and half-grabens due to tensional forces, so the displacements along these faults are

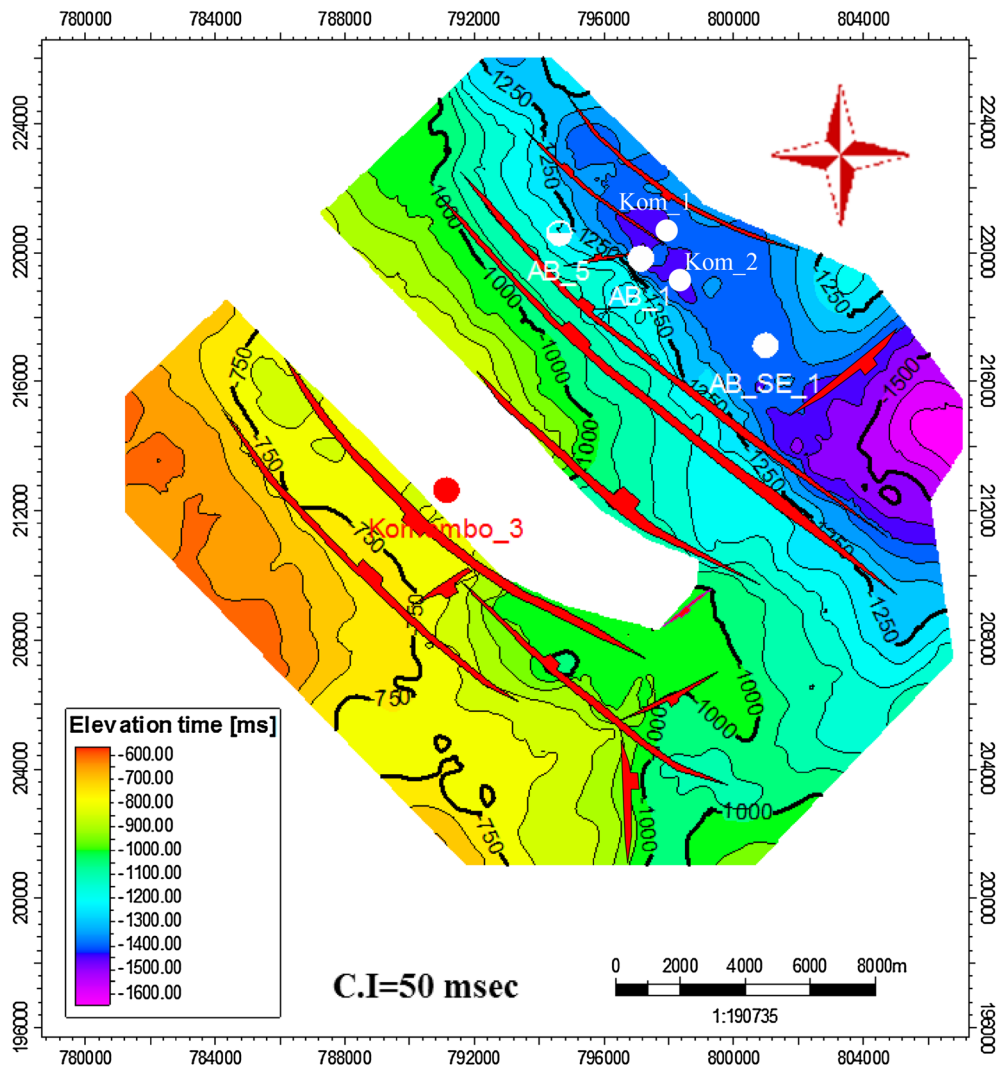


Figure 9. Two-way time contour map of the top of C Member reservoir.

reflected in the depth values of the reservoir; the maximum depth values are found in graben areas, and the minimum depth values are found in horst areas or at the shoulders of the basin. The depth values, as deduced from the 2D seismic lines, range between 2195 and 2377 m in the central and eastern parts (the depocenter of the basin) and between 914 and 1036 m in the western and southwestern parts of the Komombo Basin (the shoulders of the basin). It is not appeared in the central part of the basin and is absent in the Kom-3 well probably due to structural Paleo-highs (horst

block), and it appeared again toward the SW direction from Kom-3 well (Fig. 10).

The isopach map of the C Member reservoir was constructed by subtracting the depth map of the B member from the depth map of the C Member reservoir. Figure 11 shows that the minimum value thickness of the reservoir is 91.5 m in the southern, western and northern parts (due to the presence of the shoulders of the basin or horst structures). Meanwhile, the maximum value of the reservoir's thickness is 426.5 m in the eastern part of the Komombo Basin (due to the presence of the

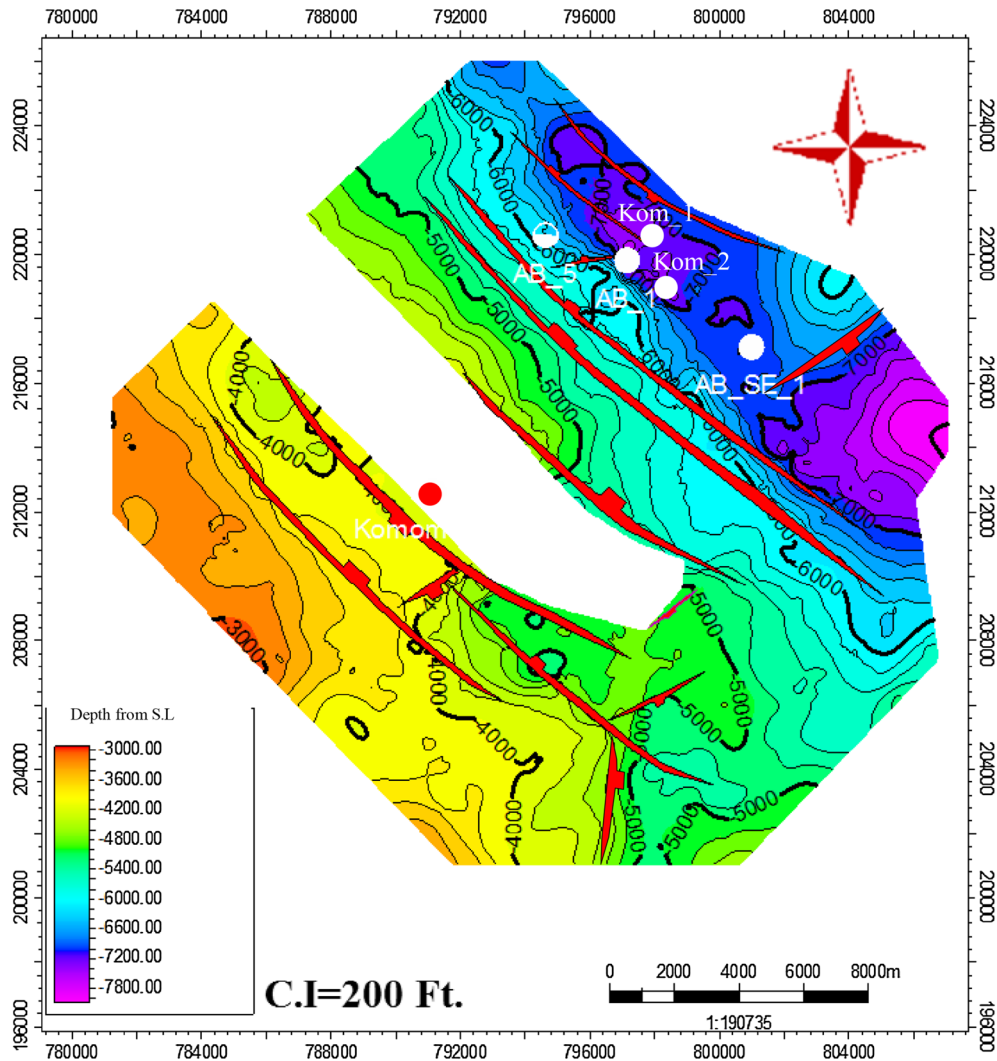


Figure 10. Depth structure contour map of the top of C Member reservoir. (1 ft = 0.3048 m).

depocenter of the basin). The large variation in the thickness of the reservoir may be related to the effect of the normal faults.

### 3D Structural Model

The 3D structural model of the C Member is necessary for the elucidation and understanding of the structural setting of the reservoir in 3D pattern. The objective is to construct a reliable structural model utilizing only a few wells by maximizing the

information from seismic data. Some cross sections are extracted from the 3D model in order to provide a clear image about the different structural features. The 3D structural model and the associated sections indicate that the dominant fault system in the Komombo Basin is represented by normal faults with a NW–SE trend (Fig. 12). Most of these faults are characterized by steep planes at the top parts with dip angle of 60°–80°, while the lower parts of the most of them have low-to-medium dip angles (20°–40°), and most of them are listric faults. The displacement values of most of these faults range be-

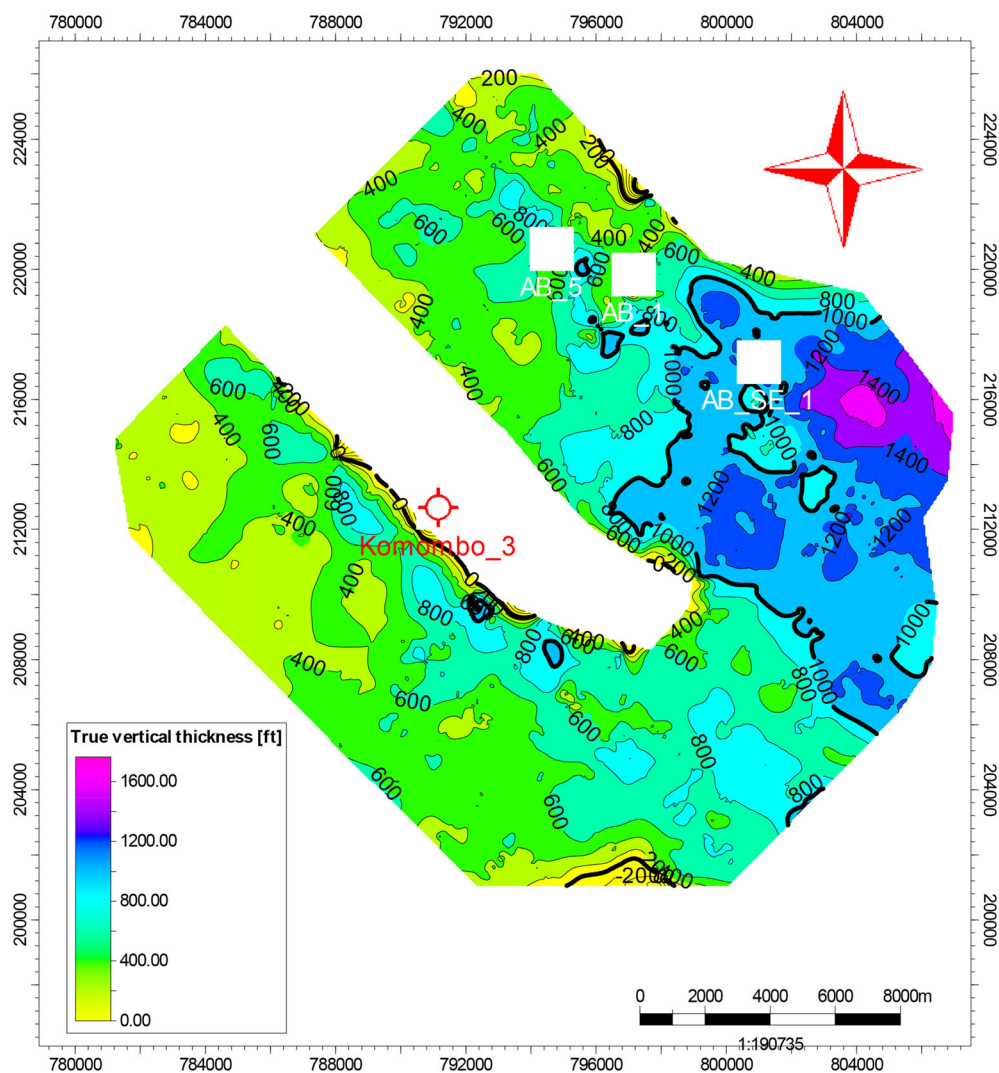


**Figure 11.** Isopach contour map of the C Member reservoir (1 ft = 0.3048 m).

tween 12 and 61 m in the SE and NW directions, forming many horst, graben and half-graben structures. Some of these faults have large displacement values ranging from 30.5 to 244 m (Ali et al. 2019a). The NW–SE and NE–SW normal faults resulted from the Early Cretaceous extension phase in the N35° E and N45° W directions, respectively, during the active opening of the South and equatorial Atlantic Ocean. This opening occurred during the Early Cretaceous rifting phases due to clockwise rotation of North and Central Africa, which was

linked with the breakup of western Gondwana (Guiraud and Maurin 1992; Philobos et al. 2000; Noweir et al. 2002; Guiraud et al. 2005; Bosworth et al. 2008). Figure 12 represents the 3D structural model of the C Member reservoir and shows horizons that are dissected by many normal faults with NW–SE and NE–SW directions. Additionally, it is noticed that the depth values of the C Member reservoir reach their maximum in the eastern part of the Komombo Basin and decrease gradually toward the corners of the basin.

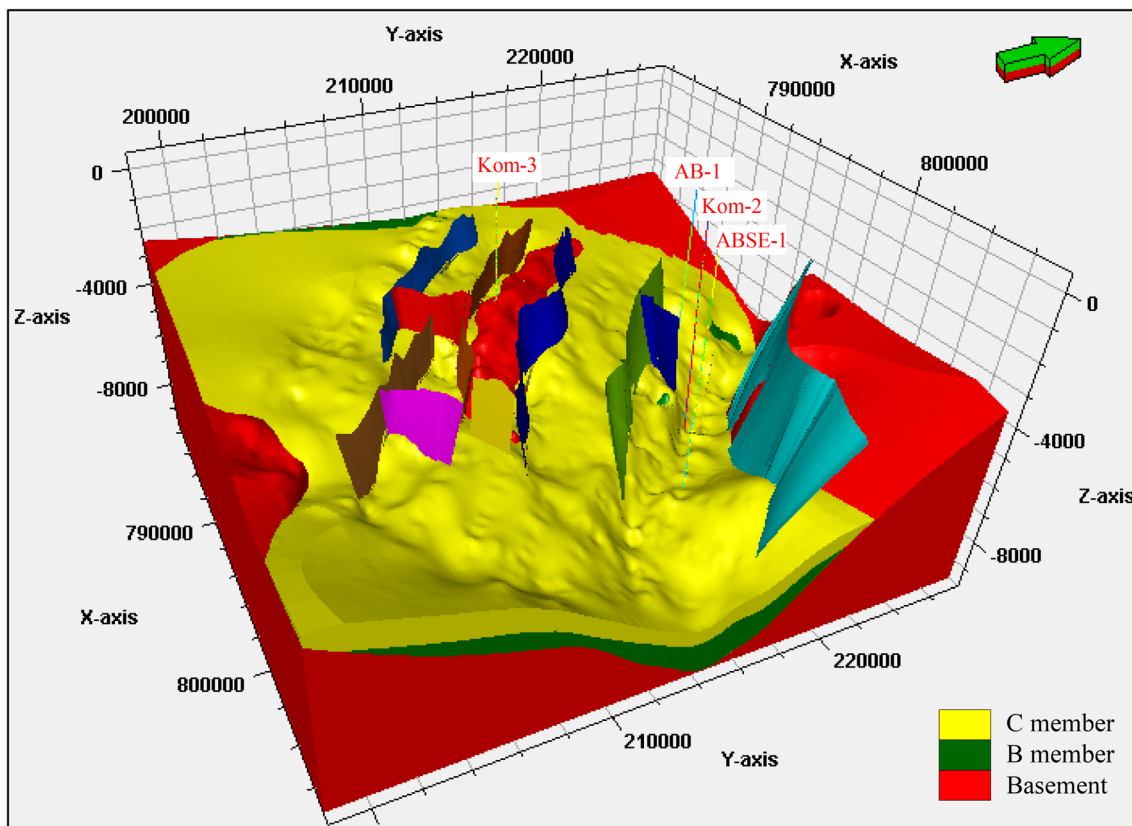


**Figure 12.** 3D C Member reservoir structure model. All faults are normal faults. Units of X- and Y-axes are in meters and Z-axis in ft (1 ft = 0.3048 m).

### 3D Facies Model

The 3D facies model of the C Member reservoir is constructed by up-scaling of the facies character for the available wells and then going through the facies modeling process. The sequential indicator simulation (SIS) algorithm is used in the facies modeling process. The 3D facies model of the reservoir shows that the shale has a large probability distribution in the study area compared to the sandstone and siltstone (Fig. 13). The C Member reservoir is composed mainly of approximately 42% shale with sandstone and siltstone at approximately 33% and 25%, respectively. The shale is concentrated in the central and northern parts of the basin, while the sandstone is concentrated in the southern part. Most of the siltstone is distributed in the northeastern part of the Komombo Basin (Fig. 13). Lateral and vertical facies change through the

studied reservoir are noticed as well. The 3D facies model of the reservoir is consistent with the interpretation of depositional systems of the Komombo Basin by Selim (2016). He supposed that the C Member of the Six Hills Formation is represented by distal braid-plain and mid-braid-plain, depending on sand/shale ratios. The distal braid-plain is composed mainly of massive to laminated, red mudstone with some medium- to coarse-grained sandstone. These sandstone facies are arranged in erosively based fining-upward pattern. The mid-braid-plain consists of semi-equal ratio of massive to laminated, red mudstone and coarse-grained sandstones. The description of the ditch samples and the patterns of the gamma ray logs of the four wells are consistent with this interpretation because the lithology shows fining-upward sequences (FUS) with shale dominating the upper part of the depositional cycle and semi-equal ratio between sandstone and mudstone

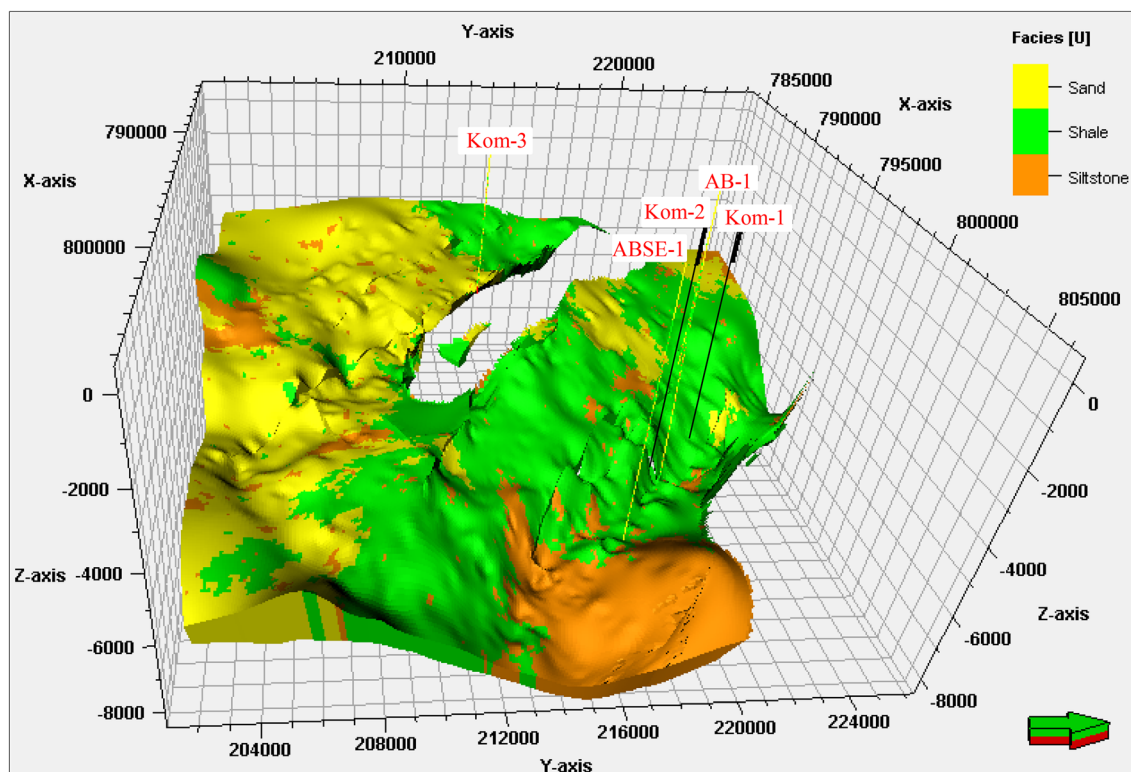


**Figure 13.** 3D facies model showing the facies distribution of the C Member reservoir. Units of X- and Y-axes are in meters and Z-axis in ft (1 ft = 0.3048 m).

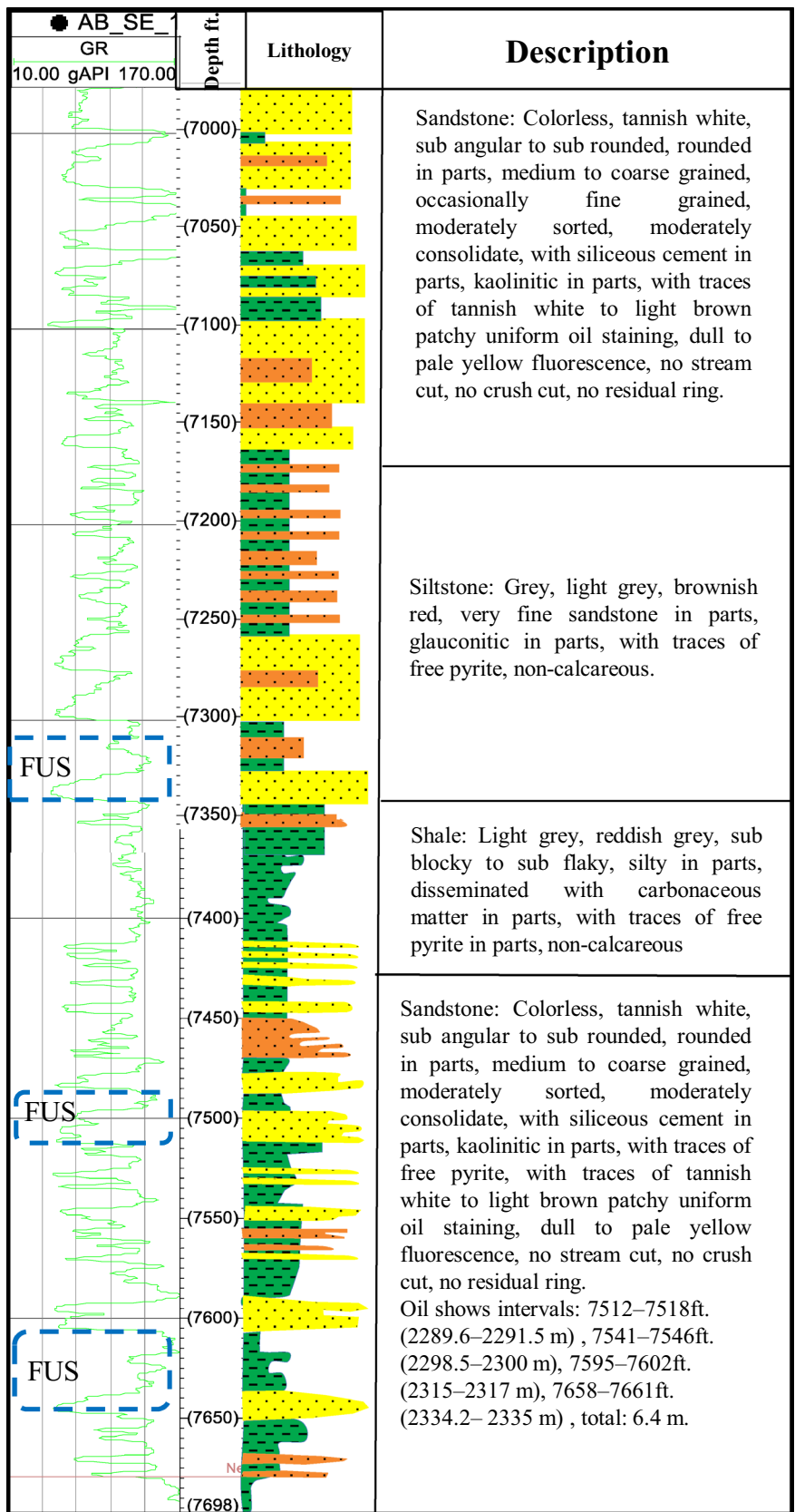
at the lowermost part of the same cycle (Fig. 14a and b). Four cross sections were extracted from the 3D facies and structural models in the N–S, E–W, NE–SW and NW–SE directions, which display the detailed lithology and structural elements of the C member reservoir (Fig. 15).

### 3D Petrophysical Model

The petrophysical parameters, obtained from the Interactive Petrophysics™ software, are up-scaled and then modeled using the petrophysical modeling process. The statistical method used in the petrophysical modeling process is the sequential Gaussian simulation algorithm. This method is appropriate, in the present case, given the amount of available data. The modeled parameters are porosity and permeability in addition to water and hydrocarbon saturation (Figs. 16, 17). Some cross sections are extracted from these models to identify the 3D

distribution of these parameters within the basin (Fig. 18).

The petrophysical models and the associated cross sections show that the C Member reservoir is generally considered to have fair reservoir quality according to the recent classifications of Nabawy and Al-Azazi (2015) and Nabawy et al. (2018a, b). This reservoir exhibits, in general, intermediate porosity and low-to-intermediate permeability values. The C Member reservoir within the Komombo Basin exhibits high net reservoir thicknesses. In contrast, this reservoir shows low net pay values, which are, related to the high water saturation values, while the hydrocarbon saturation is restricted to some parts within the basin, especially in the depocenter of the basin. The porosity and permeability increase mainly in the central portion of the study area, locating within the main depocenter of the basin. The hydrocarbon saturations through the studied reservoir increase generally in the central portion as well. The C Member in ABSE-1, Kom-1





◀ **Figure 14.** Ditch samples' description and lithology of the C Member in ABSE-1 well, interval from 7680 to 7000 ft (2341–2134 m).

and Kom-2 wells is classified as hydrocarbon-bearing reservoir, while in well AB-1 it is classified as water-bearing reservoir, as the net pay thickness in this well is negligible. Wells Kom-1 and Kom-2 have relatively small pay zones if compared to ABSE-1 well.

### SUMMARY AND CONCLUSIONS

The present study is an attempt to get clear and detailed geological information about the C Member reservoir of the Six Hill Formation. The main

results and conclusions can be summarized as follows.

The 3D structural model of the C Member reservoir shows two normal fault directions NW–SE and NE–SW, with the dominance of the NW–SE direction. The depth values of the C Member reservoir range from 2195 to 2377 m in the central and eastern parts, to 914 and 1036 m in the western and southwestern parts of the Komombo Basin. The thickness of the C Member reservoir ranges from 914 to 1036 m in the flanks and depocenter of the basin, respectively, and it varies in the drilled wells from 165, 244, 116 and 216 m in Kom-1, Kom-2, AB-1 and ABSE-1 wells, respectively. The 3D facies model shows that the C Member reservoir is composed mainly of shale about 42% with sandstone and siltstone about 33% and 25%, respectively. The petrophysical models show that the C Member reservoir is considered generally to have fair reser-

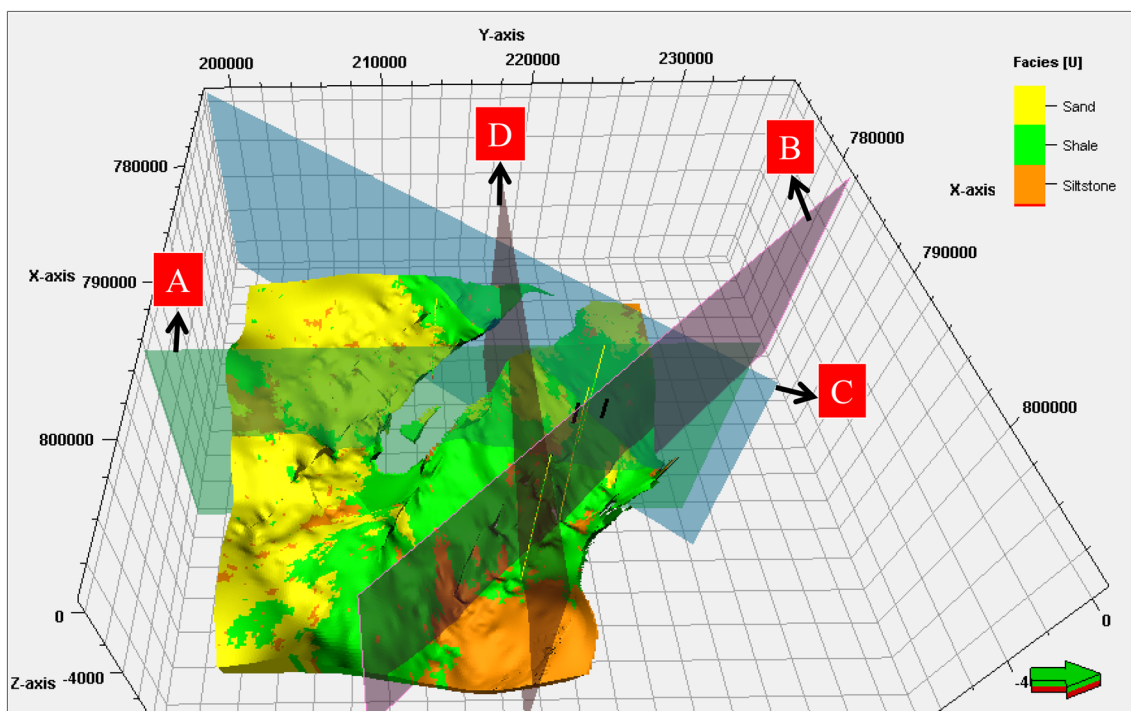


**Figure 15.** 3D facies model and the four extracted cross sections portraying the detailed lithology and structural elements of the C Member reservoir. Units of X- and Y-axes are in meters and Z-axis in ft (1 ft = 0.3048 m).

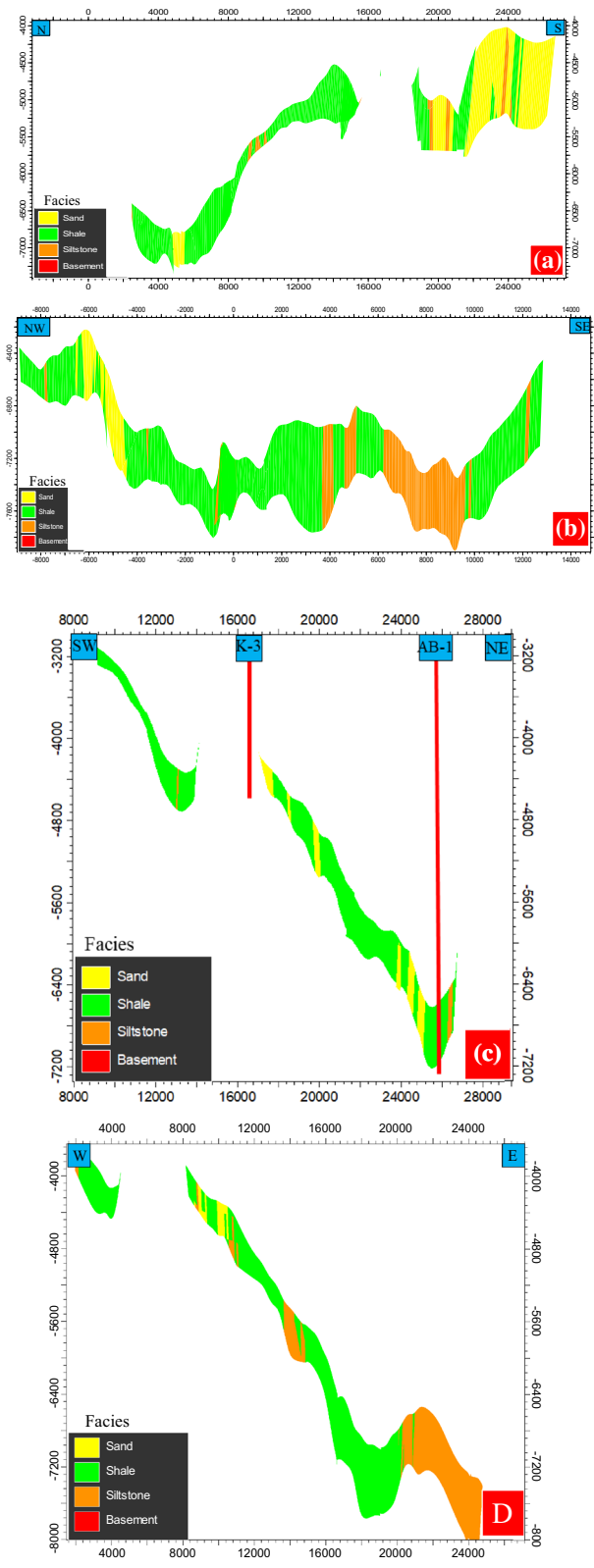


Figure 15. continued.

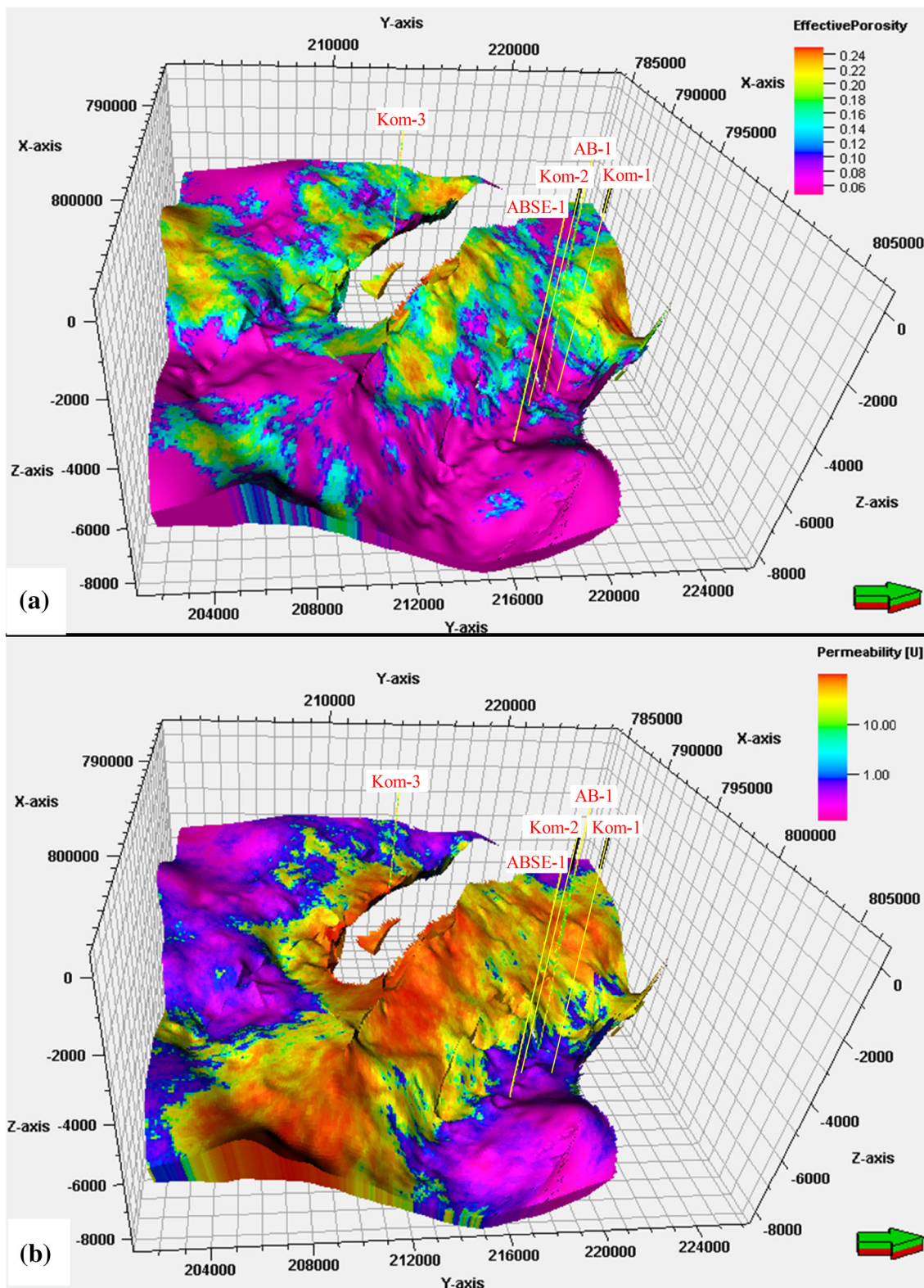


Figure 16. 3D views of the constructed petrophysical models, represented by porosity and permeability. Units of X- and Y-axes are in meters and Z-axis in ft (1 ft = 0.3048 m).

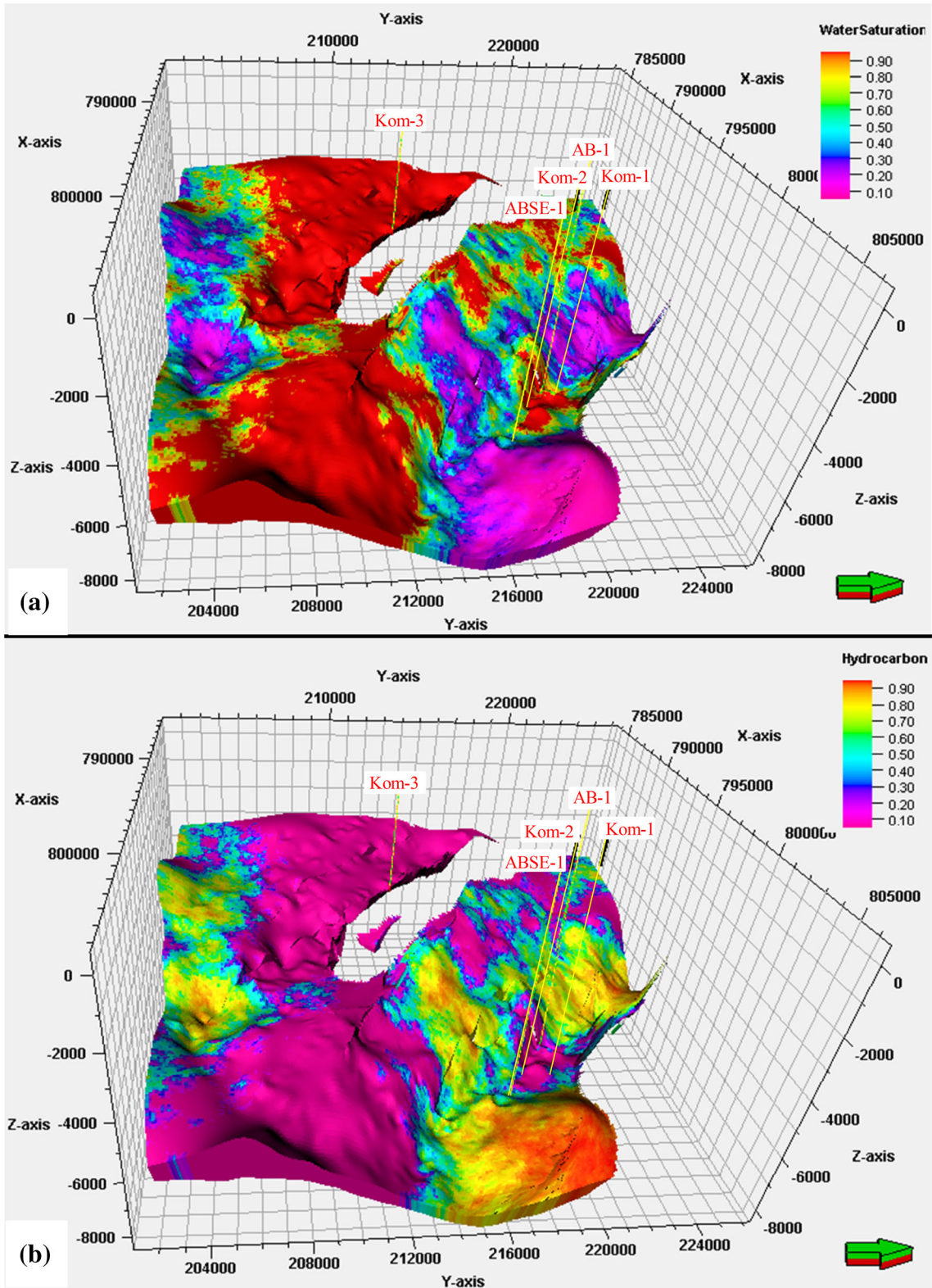
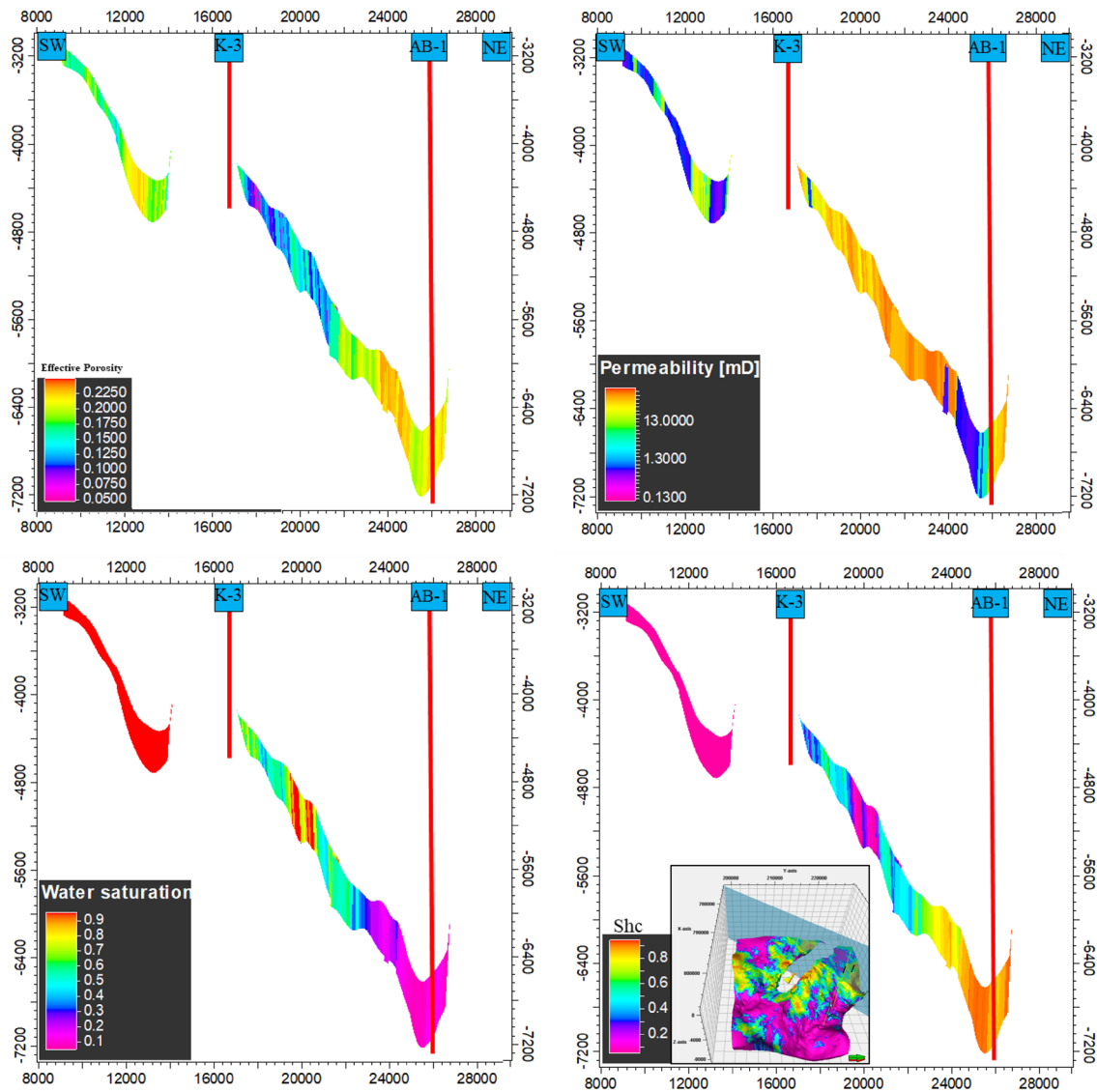


Figure 17. 3D views of the constructed petrophysical models, represented by water and hydrocarbon saturation. Units of X- and Y-axes are in meters and Z-axis in ft (1 ft = 0.3048 m).



**Figure 18.** Cross sections through the different petrophysical models in NE-SW direction. Units of X-axis are in meters and Y-axis in ft (1 ft = 0.3048 m).

voir quality. The reservoir exhibits, in general, intermediate porosity and low-to-intermediate permeability values. The reservoir has also, in general, high water saturation values. Most of the C Member reservoir within the Komombo Basin exhibits high water saturation values. In contrast, the hydrocarbon saturation is restricted to the depocenter of the basin. The porosity and permeability increase mainly in the central portion of the study area, locating within the main depocenter of the basin. The hydrocarbon saturations through the studied reservoir increase generally in the central portion as

well. In the ABSE-1, Kom-1 and Kom-2 wells, the C Member is classified as hydrocarbon-bearing reservoir; however, in the AB-1 well, it is classified as water-bearing reservoir, exhibiting very small thickness of net pay.

**ACKNOWLEDGMENTS**

The authors would like to acknowledge GANOPE Company for providing the seismic and well

data and for giving the approval to publish this manuscript. The authors are grateful to Eng. Ahmed Samy (geophysicist at GANOPE) for fruitful discussion that led to a better understanding of many points. Thanks are also due to the reviewers for their valuable comments and constructive modifications that greatly enhanced the manuscript. In addition, the authors would like to thank the Editor-in-Chief Prof. Dr. John Carranza for his effort in editing the manuscript.

## REFERENCES

- Abdel-Fattah, M., Dominik, W., Shendi, E., Gadallah, M., & Rashed, M. (2010). 3D integrated reservoir modelling for upper safa gas development in Obaiyed field, Western Desert, Egypt. In *72nd EAGE conference and exhibition incorporating SPE EUROPEC, Spain*.
- Abdelhady, A. (2016). *Hydrocarbon potential and petroleum occurrence in Komombo Sedimentary Basin, South West Nile Valley, Upper Egypt*. Ph.D. Thesis, Faculty of Science, Cairo University, Egypt.
- Abdelhady, A., Darwish, M., El-Araby, A., & Hassouba, A. (2016). Evaluation of Neocomian shale source rock in Komombo Basin, Upper Egypt. *IJSET—International Journal of Innovative Science, Engineering & Technology*, 3(1), 376–382.
- Abdelmaksoud, A. (2017). *Integrated geological modelling of the Upper Bahariya Reservoir in Abu Gharadig oil and gas field, North Western Desert, Egypt*. M.Sc. Thesis, Faculty of Science, Assiut University, Egypt.
- Abdelmaksoud, A., Amin, A. T., El-Habaak, G. H., & Ewida, H. F. (2019a). Facies and petrophysical modelling of the Upper Bahariya Member in Abu Gharadig oil and gas field, north Western Desert, Egypt. *Journal of African Earth Sciences*, 149(C), 503–516.
- Abdelmaksoud, A., Ewida, H. F., El-Habaak, G. H., & Amin, A. T. (2016). Structural style of Abu Roash “G” Member in Abu Gharadig oil and gas field, north Western Desert, Egypt, as inferred from seismic data interpretation. In *Fifth international conference for young scientists in basic and applied sciences, Assiut University, Egypt*.
- Abdelmaksoud, A., Ewida, H. F., El-Habaak, G. H., & Amin, A. T. (2017). Seismic interpretation of Abu Roash “G” Member, in Abu Gharadig oil and gas field, north Western Desert, Egypt. *Journal of Basic and Environmental Sciences*, 4(2), 107–117.
- Abdelmaksoud, A., Ewida, H. F., El-Habaak, G. H., & Amin, A. T. (2019b). 3D structural modelling of the Upper Bahariya Member in Abu Gharadig oil and gas field, North Western Desert, Egypt. *Journal of African Earth Sciences*, 150(C), 685–700.
- Abu El Ella, N. (2006). *Biostratigraphy and lithostratigraphy of Komombo-1, Komombo-2, Komombo-3, Nuqra-1 and Kharit-1 Wells, Upper Egypt*. Earth Resources Exploration (EREX), Unpublished internal report, Cairo.
- Abu El Ella, N. (2011). *Biostratigraphic studies for the AlBaraka Oil Field, Upper Egypt*. Earth Resources Exploration (EREX), Unpublished internal report, Cairo.
- Ali, M. (2017). *Tectonostratigraphy and petroleum system analysis of Al Baraka Oil Field, Komombo Basin, South Western Desert, Egypt*. M.Sc. Thesis, Faculty of Science, Assiut University, Egypt.
- Ali, M., Abdelhady, A., Abdelmaksoud, A., Darwish, M., & Essa, M. A. (2019a). 3D static modelling and petrographic aspects of the Albian/Cenomanian reservoir, Komombo Basin, Upper Egypt. *Natural Resources Research*. <https://doi.org/10.1007/s11053-019-09521-5>.
- Ali, M., Darwish, M., Abdelhady, A., & Essa, M. A. (2017a). Structural and lithostratigraphic evolution of Al Baraka Oil field, Komombo Basin, Upper Egypt as deduce from 2D seismic lines and well logging data. *Journal of Basic and Environmental Sciences*, 4(2), 149–169.
- Ali, M., Darwish, M., Abdelhady, A., & Essa, M. A. (2017b). Case study of seismic interpretation in Al Baraka Oil Field, Komombo Basin, Upper Egypt. In *Fifth international conference for young scientists in basic and applied sciences, Assiut University, Egypt*.
- Ali, M., Darwish, M., Essa, M. A., & Abdelhady, A. (2018). 2D seismic interpretation and characterization of the Hauterivian–early Barremian source rock in Al Baraka Oil Field, Komombo Basin, Upper Egypt. *Journal of African Earth Sciences*, 139, 113–119.
- Ali, M., Darwish, M., Essa, M. A., & Abdelhady, A. (2019b). Comparison between source rock potential of the Dakhla Formation in Komombo Basin and Gebel Duwi, Upper Egypt. *Arabian Journal of Geoscience*, 12, 613.
- Barthel, K. W., & Boettcher, R. (1978). Abu Ballas formation (Tithonian/Berriasian; Southwestern Desert, Egypt) a significant lithostratigraphic unit of the former (Nubian Series). *Mitteilungen der Bayerischen Staatssammlung für Paläontologie und historischen Geologie*, 21, 141–182.
- Bilodeau, B., De, G., Wild, T., Zhou, Q., & Wu, H. (2002). Integrating formation evaluation into earth modelling and 3D petrophysics. In *SPWLA 43rd annual logging symposium*.
- Bosworth, W., El-Hawat, A. S., Helgeson, D. A., & Burke, K. (2008). Cyrenaican “shock absorber” and associated inversion strain shadow in the collision zone of northeast Africa. *Geology*, 36, 695–698.
- Bryant, I. D., & Flint, S. S. (1993). Quantitative clastic reservoir geological modelling: problems and perspectives. In S. S. Flint & I. D. Bryant (Eds.), *The geological modelling of hydrocarbon reservoirs and outcrop analogues. International Association of Sedimentologists Special Publication*, 15, 3–20.
- Buckles, R. S. (1965). Correlating and averaging connate water saturation data. *Journal of Canadian Petroleum Technology*, 4(1), 42–52.
- Cosentino, L. (2005). Static reservoir study. In P. Barnaba (Ed.), *Encyclopaedia of hydrocarbons* (Vol. I, pp. 553–573). Italy: Marchesi Grafiche Editoriali S.p.a. [http://www.treccani.it/portale/opencvms/handle404?exporturi=/export/sites/default/Portale/sito/altre\\_aree/Tecnologia\\_e\\_Scienze\\_applicate/enciclopedia/inglese/inglese\\_vol\\_1/idro\\_vol\\_I\\_I\\_XXXVI\\_eng3.pdf](http://www.treccani.it/portale/opencvms/handle404?exporturi=/export/sites/default/Portale/sito/altre_aree/Tecnologia_e_Scienze_applicate/enciclopedia/inglese/inglese_vol_1/idro_vol_I_I_XXXVI_eng3.pdf).
- Darling, T. (2005). *Well logging and formation evaluation*. Amsterdam: Elsevier.
- De Jager, G., & Pols, R. W. (2006). A fresh look at integrated reservoir modelling software. *First Break*, 24, 75–81.
- Gübeli, A. A., Hochuli, P. A., & Wildi, W. (1984). Lower cretaceous turbiditic sediments from the Rif chain (northern Morocco)—Palynology, stratigraphy and palaeogeographic setting. *Geologische Rundschau*, 73, 1081–1114.
- Guiraud, R., Bosworth, W., Thierry, J., & Delplanque, A. (2005). Phanerozoic geological evolution of Northern and Central Africa: an overview. In: Catuneanu, O., et al. (Eds.), *Phanerozoic evolution of Africa. Journal of African Earth Sciences*, 43, 83–143.
- Guiraud, R., & Maurin, J.-C. (1992). Early Cretaceous rifts of Western and Central Africa: An overview. *Tectonophysics*, 213(1–2), 153–168.
- Hendriks, F., Luger, R., Kallenbach, H., & Schroeder, J. H. (1984). Stratigraphical and sedimentological framework of

- the Kharga-Sin El Kaddab stretch (western and southern part of the upper Nile Basin), Western Desert, Egypt. *Berliner geowissenschaftliche Abhandlungen*, 50(A), 117–151.
- Klitzsch, E. (1984). Flora and fauna from strata in southern Egypt and northern Sudan (Nubia and surrounding areas). *Berliner geowissenschaftliche Abhandlungen*, 50(A), 47–79.
- Klitzsch, E., Harms, J. C., Lejal-Nicol, A., & List, F. K. (1979). Major subdivisions and depositional environments of Nubia Strata, Southwestern Egypt. *AAPG Bulletin*, 63(6), 967–974.
- Larionov, V. (1969). *Borehole radiometry*. Moscow: Nedra.
- MDA Federal. (2004). Landsat GeoCover ETM+ 2000 Edition Mosaics. Sioux Falls, South Dakota, USGS, Tiles: N-35-20, N-35-25, N-35-30, N-36-20, N-36-25 and N-36-30. ETM-EarthSat MrSID.
- Meshref, W. M. (1990). Tectonic framework. In R. Said (Ed.), *The geology of Egypt* (pp. 113–156). Rotterdam: A.A. Balkema.
- Nabawy, B. S., & Al-Azazi, N. A. S. A. (2015). Reservoir zonation and discrimination using the routine core analyses data: the Upper Jurassic Sab'atayn sandstones as a case study, Sab'atayn Basin, Yemen. *Arabian Journal of Geosciences*, 8(8), 5511–5530.
- Nabawy, B. S., Basal, A. M. K., Sarhan, M. A., & Safa, M. G. (2018a). Reservoir zonation, rock typing and compartmentalization of the Tortonian–Serravallian sequence, Temsah Gas Field, offshore Nile Delta, Egypt. *Marine and Petroleum Geology*, 92, 609–631.
- Nabawy, B. S., Rashed, M. A., Mansour, A. S., & Afify, W. S. M. (2018b). Petrophysical and microfacies analysis as a tool for reservoir rock typing and modeling: Rudeis Formation, offshore October Oil Field, Sinai. *Marine and Petroleum Geology*, 97, 260–276.
- Nagati, M. (1986). Possible mesozoic rift in Upper Egypt: An analogy with the geology of Yemen–Somalia rift basins. In *4th Exploration and production conference, EGPC, Cairo, Egypt*.
- Noweir, A. M., Noweir, A. S., Nassm, A. S., Lebda, E. M., & El-Kholify, E. M. (2002). Late Cretaceous transpression—Tertiary extension affecting the Phanerozoic sedimentary formations, east Kom Ombo south Eastern Desert, Egypt. *Middle East Research Centre, Ain Shams University, Earth Science Series*, 16, 145–165.
- Philobos, E., Riad, S., Omran, A. A., & Othman, A. B. (2000). Stages of fracture development controlling the evolution of the Nile Valley in Egypt. *Egyptian Journal of Geology*, 44, 503–532.
- Pickett, G. R. (1972). *Practical formation evaluation*. Golden Colorado: GR Pickett Inc.
- Poupon, A., & Leveaux, J. (1971) Evaluation of water saturation in shaly formations. In *Proceedings of the SPWLA 12th annual logging symposium*.
- Schrank, E. (1991). Mesozoic palynology and continental sediments in NE Africa (Egypt and Sudan)—A review. *Journal of African Earth Sciences*, 12, 363–373.
- Schrank, E. (1992). Nonmarine cretaceous correlations in Egypt and northern Sudan: palynological and palaeobotanical evidence. *Cretaceous Research*, 13, 351–368.
- Selim, S. S. (2016). A new tectono-sedimentary model for cretaceous mixed nonmarine–marine oil-prone Komombo Rift, South Egypt. *International Journal of Earth Sciences*, 105(5), 1387–1415.
- Taha, M. A., & Aziz, H. (1998) Mesozoic rifting in Upper Egypt concession. In *14th International petroleum conference* (p. 5) (abstract).
- Timur, A. (1968). An investigation of permeability, porosity and residual water saturation relationships for sandstone reservoirs. In *SPWLA 9th annual logging symposium, New Orleans, Louisiana* (Vol. 9, p. 4).
- Wycisk, P. (1987). Contribution to the subsurface geology of the Misaha trough and the southern Dakhla Basin (S. Egypt/N. Sudan). *Berliner geowissenschaftliche Abhandlungen*, 75(A), 137–150.
- Ziegler, P. A. (1992). Geodynamics of rifting and implications for hydrocarbon habitat. *Tectonophysics*, 215, 221–253.